Galactic Halos: A UC Santa Cruz Workshop
ASP Conference Series, Vol. 136, 1998
Dennis Zaritsky (ed.)

Damped Lyα Systems: The Progenitors of Galaxy Disks

A. M. Wolfe[1]
Department of Physics and CASS, University of California, San Diego
La Jolla, CA 92093-0424

Abstract. I describe measurements of the kinematics of gas in damped Lyα systems which discriminate among competing theories for galaxy formation. Low-ion velocity profiles obtained with the HIRES echelle spectrograph of the Keck I telescope exhibit multi-component structures spanning velocity intervals Δv = (20,290) km s^{-1}. The velocity components exhibit "edge-leading" asymmetries in which the strongest component is at the edge of the profile. Other than rapidly rotating thick disks, all scenarios *we tested* with Monte Carlo techniques are inconsistent with the data. There are sufficient baryons in the metal-rich damped Lyα systems to explain the formation of the thick stellar disks seen in current spirals. We describe tests that can discriminate between rapidly rotating disks and the protogalactic clumps predicted by CDM models.

1 Introduction

In this paper I focus on high-redshift objects that are the probable progenitors of galaxy disks. The objects I have in mind are the damped Lyα absorption systems, a population of H I layers detected in absorption against background quasars. Because of their large H I column densities, N(H I) $\geq 2\times10^{20}$cm^{-2}, the gas is neutral which sets them apart from all other classes of quasar absorption systems in which the gas is ionized (Wolfe 1993).

The damped systems have attracted considerable attention for the following reasons:

• They dominate the H I content of the universe in the redshift interval z =(0,4.5).

• The comoving density of neutral gas, $\Omega_g(z)$, changes with time (see Figure 1). It *increases* with time by a factor of 3 from $z = 4.5$ to 3.3, is nearly constant from $z = 3.3$ to 1.8, and decreases with time from $z = 1.8$ to 0.75.

• In the redshift interval z = (1.8,3.3) $\Omega_g(z)$ peaks and is comparable to Ω_{star}, the density of visible matter in current galaxies. Thus, there are sufficient baryons in gas at high redshift to account for the mass content of visible stars at present. As $z \rightarrow 0$, $\Omega_g(z)$ approaches Ω_{21}, the density of neutral hydrogen inferred from unbiased surveys for 21 cm emission (Briggs 1997). Because 90 %

[1]Visiting Astronomer, W. M. Keck Telescope. The Keck Observatory is a joint facility of the University of California and the California Institute of Technology

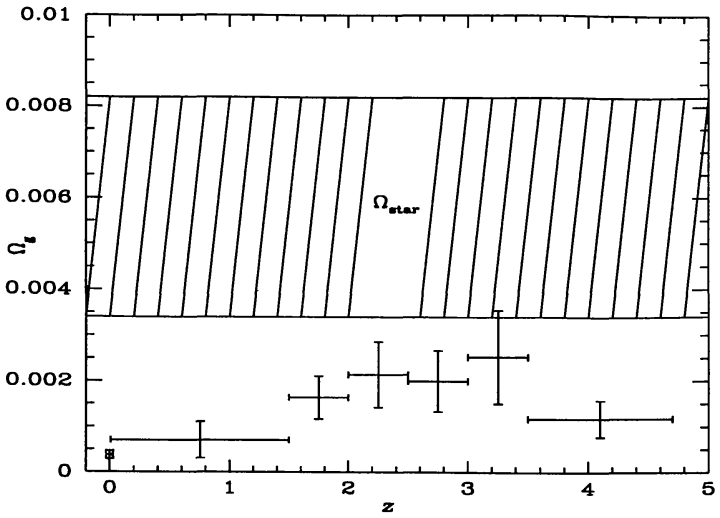

Figure 1. Comoving density of neutral gas vs redshift. Points at $z \neq 0$ inferred from damped Lyα statistics for Ω_0=1,Λ=0,h=0.5 (Storrie-Lombardi & Wolfe 1997). Data point at $z = 0$ inferred from 21 cm surveys (Briggs 1997). Horizontal lines are $\pm$ 1σ contours of density of visible matter.

of Ω_{21} is located in luminous spirals, the same galaxies dominating Ω_{star}, it is reasonable to assume that $\Omega_g(z)$ traces the evolution of the neutral gas content of massive galaxies from their protogalactic phase to the present.

However, we are a long way from understanding the sequence of events leading from gas-rich protogalaxies to current galaxies of stars. The most widely accepted scenario is the hierarchical CDM cosmology in which the ancestors of current massive spirals are low-mass subunits that evolve by a series of merger events into massive galaxies. There are two versions of this model. The first comprises semi-analytic models (White & Frenk 1991; Kauffmann 1996; Mo, Mao, & White 1997) in which the low-mass subunits consist of gas bound to dark matter halos. The gas collapses and spins up to form rotating disks, with rotation speeds $v_{rot} \sim 100$ km s^{-1}, in centrifugal equilibrium with halo masses $\sim 10^{10}$ M$_\odot$. Mergers between disks lead to spheroidal bulge-like structures rather than disks. The second version is the protogalactic clump model which emerged from a numerical simulation of gas and dark matter in a CDM cosmology. Since the collapse time in individual halos is long compared to the merger time scale, rotating disks in low-mass halos never form in this model (Haehnelt et al. 1997). Rather, infall, random motions, and rotation make comparable contributions to the velocity field at $z > 2$. In both scenarios, current rapidly rotating disks do not form until $z < 1$.

The competing model is the monolithic collapse scenario (Eggen et al. 1962). The idea is that the current mass distribution of galaxies was in place at $z > 5$. Gas initially at the virial temperature of $\sim 10^6$ K cools, collapses, and spins up to form the galaxies we see today. Because of the short collapse time, disks with the current rotation speeds are in place at $z \sim 5$. This model has been set in a cosmological context by Peebles (1997).

In this paper I show how measurements of the kinematics of the gas help to discriminate among these scenarios. In particular I describe how the velocity profiles of low-ion metal-lines in damped systems exhibit properties that rule out the semi-analytic models and most other models suggested to explain the damped systems (§ 2). The only successful models *we tested* are those incorporating rapidly rotating, thick disks, consistent with the monolithic collapse scenario. In § 3 I show how star formation in such disks leads naturally to the formation of the current thick stellar disk. In § 4 I compare the merits of the protogalactic clump model and the rapidly rotating disk model.

2 Low-ion Kinematics

To obtain kinematic information, Jason X. Prochaska, a graduate student at UCSD, and I have used the HIRES echelle spectrograph (Vogt 1992) on the Keck I 10 m telescope to acquire accurate velocity profiles of low-ion transitions. We focus on transitions such as Si II 1808 and Ni II 1741, because Ni^+ and Si^+ trace the velocity field of the neutral gas. The data typically have velocity resolution with FWHM = 7 km s^{-1} and signal-to-noise ratio of 30:1. We now have velocity profiles for 31 damped systems. Figure 2 plots the apparent optical depth, τ, vs velocity for all 31 profiles, where $\tau \equiv -\ln[I(v)]$ and $I(v)$ is intensity at velocity v normalized to unit quasar continuum. The profiles in Figure 2 show (a) the gas is distributed among discrete, narrow velocity components, (b) the strongest component is at either edge of the profile in 19 out of 22 cases in which the velocity interval $\Delta v > 40$ km s^{-1}, and (c) the profile widths are in the range $\Delta v = (20,290)$ km s^{-1}.

The "edge-leading" asymmetries of the profiles in Figure 2 bring to mind similar asymmetries exhibited by absorption profiles arising in the ISM (Savage & Sembach 1996). Thus, it is natural to assume the profiles in Figure 2 are generated by passage of the line of sight through a disk with (a) constant rotation speed, v_{rot}, and (b) gas density $n(R,z) \propto \exp[-(R/R_d)-(|z|/h)]$ where R_d and h are radial scale-length and vertical scale-height. The strongest absorption normally occurs where the line of sight encounters the disk at midplane; i.e., $z = 0$. The absorption profile trails off with velocity as the cloud density decreases with increasing $|z|$ (see Prochaska & Wolfe 1997). The profile widths are determined by angle of inclination of the disk and by the impact parameter, b, of the sightline relative to the center of the disk.

We test the disk hypothesis with Monte-Carlo models. We let sightlines penetrate the midplanes of *identical*, randomly oriented, exponential disks at random locations. Clouds with internal velocity dispersion, σ_{int}, are randomly drawn from the $n(R,z)$ distribution and then assigned appropriate line-of-sight velocities which are the vector sums of the projected v_{rot} and random velocities drawn from Gaussian velocity distributions internal to the clouds and external motions parameterized by the velocity dispersion σ_{cc}. We then solve the transfer equation for radiation propagating through the assembled cloud configuration. When necessary, we readjust $Nf\lambda$ in order that $I(v_{pk})$, the residual intensity of the absorption feature with peak optical depth, satisfies the condition, $0.1 < I(v_{pk}) < 0.6$. This excludes saturated absorption features and guarantees the

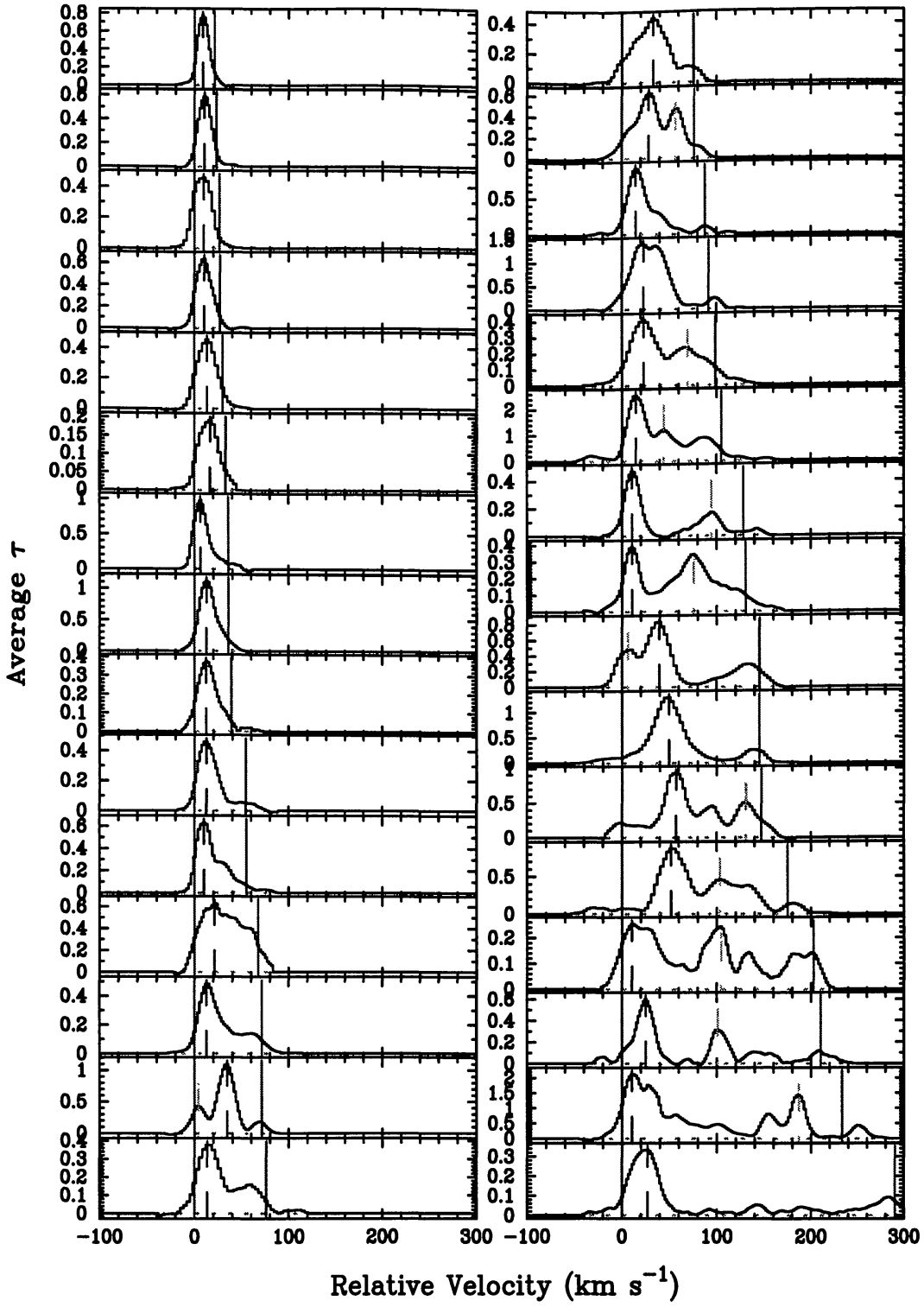

Figure 2. Velocity profiles of low-ion metal lines for 31 damped Lyα systems. Data obtained from Keck I telescope with HIRES echelle spectrograph at FWHM resolution of $\sim$ 7 km s^{-1}. Data binned in intervals of $\sim$ 10 km s^{-1}.

detection of weak features necessary for detecting profile asymmetries. We also adopt algorithms specifying the number of clouds along the line of sight.

We also consider other models with disks. The most important of these is the semi-analytic CDM model in which v_{rot} is drawn from an interception-probability distribution computed by Kauffmann (1996). Configurations without disks include clouds orbiting at the virial velocities of halos of massive galaxies (Lu et al. 1996), and spherical infall models. Each model is tested by comparing synthetic and empirical distributions of test statistics. The test statistics are low-order moments of the profiles such as Δv and higher order moments that test the asymmetries of the profiles such as $|v_{mean} - v_{median}|/(\Delta v/2)$ where v_{mean} and v_{median} are the mean and median velocities of the profiles. Using two-sided KS tests we rule out all models we considered other than rapidly rotating disks. Because most of the disks in the semi-analytic CDM model are rotating with $v_{rot} < 100$ km s^{-1}, this model does not reproduce the significant number of profiles with $\Delta v > 100$ km s^{-1}. The halo model fails because it cannot reproduce the detected edge-leading asymmetries and because the Δv distribution peaks at velocities much greater than the maximum $\Delta v = 290$ km s^{-1}. The spherical infall models fail because they predict too many profiles with strong absorption features at both profile edges.

To learn more about the disks we constructed Likelihood functions from the Δv distributions, the distributions most sensitive to variations of the crucial parameters, v_{rot} amd h/R_d. The Likelihood contours in the v_{rot}, h/R_d plane indicate that models in which $v_{rot} < 250$ km s^{-1} and $h/R_d < 0.1$ are ruled out at the 99 % confidence level. Because the Likelihood peaks at $v_{rot} \approx 300$ km s^{-1} and $h/R_d = 0.3$, the disks must be thick as well as rapidly rotating. Current spirals with $v_{rot} = 300$ km s^{-1} are rare per unit volume, and as a result we are computing more realistic models in which v_{rot} is drawn from a suitable distribution function. We have calculated interception probability distributions from Schechter luminosity functions in which galaxy luminosity is related to v_{rot} through the Tully-Fisher relation, and in which cross-section is related to luminosity (hence v_{rot}) through the Holmberg relation, area $\propto L^{0.8}$. Monte Carlo tests of such models indicate good agreement with the tests described above.

3 Formation of the Thick Stellar Disk

I interpreted the damped Lyα systems as rapidly rotating, thick *gaseous* disks. I also argued that the cold, neutral damped Lyα gas contains sufficient baryons to account for all the visible stars in current galaxies. Therefore, it is natural to ask whether stars produced in damped Lyα systems exhibit properties compatible with known stellar populations? Stars forming out of the damped Lyα gas would be much too metal-poor to explain the thin disk (Pettini et al. 1997), and the kinematics of the gas are incompatible with the velocity structure of halo stars (see § 2). Because the mean metallicity of stars in the thick disk is higher than that of the damped systems, Pettini et al. (1997) also argued that the damped Lyα systems could not be the progenitors of the thick disk. But this possibility is worth re-examining because of the significant overlap in the two metallicity distributions; i.e., there may be sufficient baryons in the metal-rich subset of the damped systems to account for the baryonic masses of thick disks.

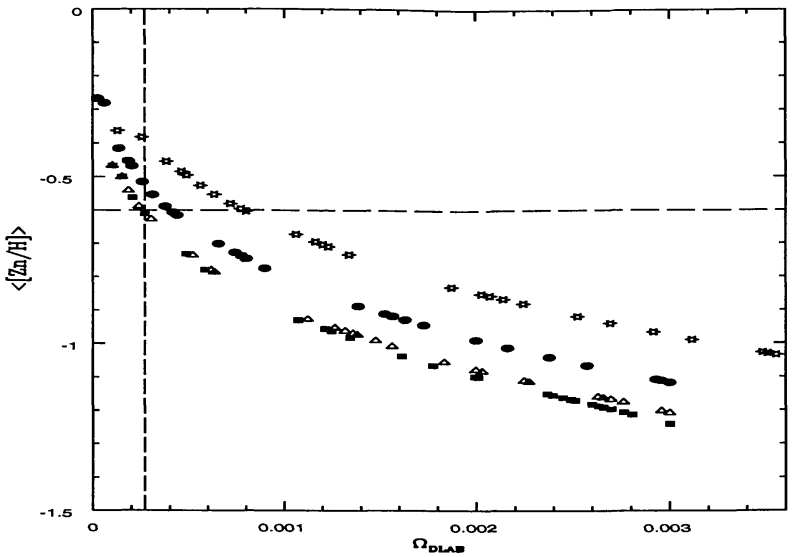

Figure 3. Mean metallicity of damped systems vs comoving density of damped Lyα baryons with metallicities $Z' = (Z, Z_{max})$. Circles assume upper limits equal true values of Zn abundances, triangles and squares computed assuming upper limits minus 0.5 and 1.0 dex equal true values of abundances. Stars include corrections for presence of baryons in stars. Vertical and horizontal dashed lines correspond to mass density and mean metallicity of thick stellar disk.

Let the cosmic metallicity $< \mathcal{Z} > \equiv \Omega_{metals}/\Omega_g$, where Ω_{metals} and Ω_g are the comoving densities of metals and neutral gas in damped Lyα systems. Suppose the joint metallicity, column-density distribution spans the metallicity interval $Z' = (Z_{min}, Z_{max})$ and the column-density interval $N = (N_{min}, N_{max})$, and $\Omega_g(Z)$ is the comoving density of damped Lyα baryons in the metal-rich subinterval $Z' = (Z, Z_{max})$. In the discrete limit, $\Omega_g(Z)$ and the corresponding $< \mathcal{Z}(Z) >$ are given by

$$\Omega_k = \Omega_g \times \frac{\sum_{i=1}^{k} N_i}{\sum_{j=1}^{i_{min}} N_j} \quad , < \mathcal{Z}_k > = \frac{\sum_{i=1}^{k} N_i \times Z_i'}{\sum_{j=1}^{k} N_j} \quad , \tag{0.1}$$

where the indices i =1, k, and i_{min} correspond to Z_{max}, Z, and Z_{min}; i.e., the sums extend over an array of damped systems ordered by decreasing metallicity.

To determine $< \mathcal{Z}(Z) >$ as a function of $\Omega_g(Z)$ we use the Zn abundances Pettini et al. (1997) acquired for 27 damped Lyα systems in which z = (1.6,3.0). Systems with $z > 3.0$ are excluded, since the metallicities in this redshift range are systematically lower than those of the thick disk. We use equation (1) to determine the points in Figure 3 in which <[Zn/H]> ($\equiv \log(< \mathcal{Z}(Z) >/Z_\odot)$) is plotted against $\Omega_g(Z)$ for $Z = (Z_{max}, Z_{min})$. We set $\Omega_g = 0.003$, the value of $\Omega_g(z)$ for z = (1.6,3.0) and $H_0 = 50$ km s^{-1} Mpc^{-1} (see Fig. 1). The circles are computed by letting the upper limits equal the true Zn abundances. In this case $\Omega_g(Z) = 0.004$ when $\log(< \mathcal{Z}(Z) >/Z_\odot) = -0.6$, the mean metallicity of the thick disk (Carney et al. 1996). The triangles and squares are computed by letting the upper limits minus 0.5 and 1.0 dex equal the true Zn abundances, and in this case the critical $\Omega_g(Z) = 0.003$, indicating the result is robust. Because

of evidence for the presence of stars in the most metal-rich damped systems, and since metals in stars as well as gas are sources of metals in current thick stellar disks, we modified eq. (1) to calculate <[Zn/H]> as a function of $\Omega_{baryon}(Z)$ when metals and baryons in stars are included. Here $\Omega_{baryon}(Z)$ is the comoving density of baryons in stars and gas for metallicities $Z' = (Z, Z_{max})$. In this case $\Omega_{baryon}(Z) = 0.008$ when $\log(< \mathcal{Z}(Z) >/Z_{\odot}) = -0.6$ (see Wolfe & Prochaska 1998 for details). By comparison we estimate the cosmic mass density of thick stellar disks, $\Omega_{thick} = 0.00027$. I conclude the damped systems contain sufficient baryons to account for the masses of thick stellar disks.

4 Rotating Disks and Protogalactic Clumps

Haehnelt et al. (1997) computed a numerical CDM gas-dynamical simulation of galaxy formation with spatial resolution of 1 kpc. They used the velocity and density structure of the gas to generate velocity profiles of low-ion absorption lines in damped Lyα systems. Using the formalism of Prochaska & Wolfe (1997) they generated distributions of test statistics computed from the profiles (see § 2). Although the halo masses and circular velocities, $v_c = \sqrt{GM(r)/r}$, were similar to those predicted by the semi-analytic model (Kauffmann 1996), the kinematic properties of the models differed in that the KS tests ruled out the semi-analytic model at high significance levels (Prochaska & Wolfe 1997), but did not rule out the numerical models.

The two CDM models predict different kinematics for the following reasons. In the semi-analytic model the time scale for mergers between halos is long compared to the time scale for collapse of gas in a halo, while the reverse is true in the numerical simulation. As a result, the simulation does not predict the presence of centrifugally supported disks in equilibrium with the halo gravitational field. Rather, the gas and dark matter are confined to protogalactic clumps, and in contrast to the semi-analytic model, infall, random motions and rotation make comparable contributions to the velocity field. The last point is important since sightlines traversing such configurations sample larger velocity gradients than sightlines traversing rotating disks. For example, Haehnelt et al. (1997) find that $\Delta v_{median} = 0.6 v_c$ for the protogalactic clump model, while $\Delta v_{median} = 0.3 v_c$ for rotating disks, where Δv_{median} is the median profile velocity width. This explains why the protogalactic clump model is more successful than the semi-analytic model in explaining the observed Δv distribution. The protogalactic clump model also reproduces the "edge-leading" velocity asymmetry discussed in § 2. Clumps with the highest volume density and column density experience the lowest ram-pressure acceleration from the surrounding gas flow. As a result, the strongest absorption features appear at the profile edges.

Thus, rapidly rotating disks predicted by monolithic collapse and protogalactic clumps predicted by CDM cosmologies are compatible with the kinematic tests discussed by Prochaska & Wolfe (1997). I can think of other tests that potentially distinguish between these scenarios. First, in § 3 I showed that monolithic collapse predicts formation of the thick stellar disks at redshifts $z =$ 2 to 3. By contrast, stellar disks form at $z < 1$ in hierarchical cosmologies (Mo et al. 1997). But the age of the thick disk is comparable to the ages of the metal-

rich globular clusters, which are greater than 12 Gyr (Carney priv. comm.). This exceeds the look-back time to $z = 1$ in all $\Omega_\Lambda = 0$ cosmologies and spatially flat cosmologies in which $\Omega_\Lambda < 0.8$, when $H_0 > 50$ km s^{-1} Mpc^{-1}. Thus, the thick disks predicted by the protogalactic clump model may be too young. Second, the distribution of impact parameters, b, separating sightlines through damped Lyα systems from the brightness centroids of associated galaxies differ in the two models. Whereas the median b for the protogalactic clump scenario is ~ 3 kpc, Storrie-Lombardi & Wolfe (1997) show the median $b \sim 20$ kpc for disks that (1) create damped Lyα systems and (2) have the comoving density of normal galaxies. The corresponding angular diameters, $\theta_b \approx 0.5$ arcsec and 2.5 arcsec for objects with $z \approx 3$. Djorgovski (1997) detected two galaxies associated with damped Lyα systems with $z = 3.15$ and 4.1 with $\theta_b \approx 2.3$ and 3.3 arcsec. Such large impact parameters are consistent with the larger disks predicted by monolithic collapse. However, a larger sample of impact parameters, including upper limits resulting from null detections, is needed to construct the *distribution* of impact parameters required for deciding between the hypotheses.

Acknowledgments. I wish to thank my collaborators Jason Prochaska and Lisa Storrie-Lombardi for permission to report on our unpublished results. Partial support was received from NASA grant NAGW-2119 and NSF grant AST 86-942044.

References

Briggs, F. H. 1997, astro-ph/970549

Carney, B. W., Laird, J. B., Lathan, D. W., & Aguilar, L. A. 1996, AJ 112, 668

Djorgovski, S. G. 1997, astro-ph/9709001

Eggen, O. J., Lynden-Bell, D., & Sandage, A. R. 1962, ApJ 136, 748

Haehnelt, M. G., Steinmetz, M., & Rauch, M. 1997, astro-ph/9706201

Kauffmann, G. 1996, MNRAS 281, 475

Lu, L., Sargent, W. L. W., Barlow, T. A., Churchill, C. W., & Vogt, S. S. 1996, ApJS 107, 476

Mo, H. J., Mao, S., & White, S. D. M. 1997, astro-ph/9707093

Peebles, P. J. E. 1997, ApJ 483, L1

Pettini, M., Smith, L. J., King, D. L., & Hunstead, R. W. 1997, ApJ 486, 665

Prochaska, J. X., & Wolfe, A. M. 1997, ApJ 487, 73

Savage, B. D. & Sembach, K. R. 1996, ApJ 470, 893

Storrie-Lombardi L. J., & Wolfe, A. M. 1997, in preparation

Vogt, S. S. 1992, in ESO Conf. and Workshop Porc 40, High Resolution Spectroscopy wit the VLT, ed. M. -H. Ulrich, Garching: ESO, 22

White, S. & Frenk, C. 1991, ApJ 38, 357

Wolfe, A. M. 1993, in Relativistic Astrophysics and Particle Cosmology, ed. C. W. Akerlof & M. A. Srednicki, New York: New York Academy of Sciences, 281

Wolfe, A. M., & Prochaska, J. X. 1998, ApJ, accepted for publication